JOURNAL OF Materials CHEMISTRY

Boron-doping effects in carbon nanotubes

Wen K. Hsu,[a] Steven Firth,[b] Philipp Redlich,[c] Mauricio Terrones,[c,d] Humberto Terrones,[a,d] Yan Q. Zhu,[a] Nicole Grobert,[a] Andreas Schilder,[e] Robin J. H. Clark,[b] Harold W. Kroto[a] and David R. M. Walton[a]

[a]*School of Chemistry, Physics and Environmental Science, University of Sussex, Brighton, UK BN1 9QJ*
[b]*Christopher Ingold Laboratories, Chemistry Department, University College London, 20 Gordon St, London, UK WC1H 0AJ*
[c]*Max Planck Institut für Metallforschung, Seestr 92, D-70174 Stuttgart, Germany*
[d]*Instituto de Fisica, UNAM, Apartado Postal 1-1010, 76000 Querétaro, México*
[e]*Lehrstuhl für Experimental Physik, Universität Bayreuth und Bayreuther Institut für Makromolekülforschung, D-95440 Bayreuth, Germany*

Received 26th January 2000, Accepted 27th March 2000
Published on the Web 25th April 2000

When nanotubes form in a carbon arc, the presence of boron results in long boron-doped carbon nanotubes which are generated as dominant zigzags. Metallic behaviour is observed, in contrast to carbon nanotubes, which are semi-conducting.

1. Introduction

Boron-containing carbon fibres and allied materials have been studied widely since the 1960s, one of the initial aims being to evaluate their electronic structure.[1–3] Various measurements (*e.g.* EPR, magnetic susceptibility, resistivity, Hall effect and magnetoresistivity) have shown that the mobility of the charge carriers and the diamagnetic susceptibility of these materials are strongly dependent upon the boron concentration. Early preparative methods employed have been reviewed[4] and are generally divided into two types: (a) boron addition to carbon (i) prior to or (ii) after graphitisation; and (b) introduction of boron into an organic precursor before carbonization. A recent discovery, made during carbon arc generation of multi-walled carbon nanotubes (MWCNs), is that the carbon tubules can be efficiently lengthened when the graphite anode contains elemental boron,[5–7] and that BC_3 units, in particular, appear to be incorporated into the hexagonal carbon network.[5–7] In the arc discharge process, boron is incorporated simultaneously with graphitisation of the carbon nanotubes.

In general, the lengths of carbon nanotubes range from *ca.* 4 to 8 μm for C/arc-generated and from *ca.* 10 to 200 μm for BC/arc-generated products; the diameter (5–40 nm) is comparable in both, based on TEM and SEM observations.[5–8] Calculations suggested that the closure energy for nanotubes, which we assume involves the formation of pentagonal rings, is greater when boron is bonded to the network edges, than in the case of pure carbon nanotubes.[9] Accordingly, boron is believed to play a key role at the open end of a growing tube, particularly in controlling the structure of tube walls. In this paper, we have systematically investigated the effects of boron-doping in carbon nanotubes using TEM, EELS, X-ray diffraction, electron diffraction, Raman spectroscopy and microwave measurements.

2. Experimental

Boron-containing carbon nanotubes (BCCNs) were prepared by passage of a dc arc between a hollow graphite anode filled with BN powder, and a pure graphite cathode in a 500 Torr helium atmosphere, as described previously.[7] The BCCNs were purified by an established technique[10] utilising ultrasonic and microfiltering processes. Raw material (100 mg), extracted from the dark inner core of the cylindrical cathode deposit and ground in a mortar, was sonicated with acetone (100 cm^3) for 10 min. The mixture was transferred to a Büchner funnel fitted with a glass filter (4–10 μm porosity); this was then placed in an ultrasonic bath and connected to a vacuum. Passage of the polyhedral carbon particles, and the flake-like and amorphous carbon (suspended in acetone) through the filter was thereby achieved, leaving long nanotubes as a deposit on the surface of the filter. In this way, structural damage to the nanotubes was minimised (unlike the oxidative process,[11] which tends to cause extensive damage to the ends of the nanotubes). Although small quantities of the carbon particles and flake-like materials remained attached to the nanotubes after the process, the sample contained more than 85% nanotubes (Fig. 1). EELS measurements were made on a JEOL-2010 HRTEM instrument; X-ray powder diffraction was carried out on a SIEMENS D-5000 diffractometer, using Cu-Kα radiation. The Raman spectra of BCCNs, and a sample of MWCNs purified using the same procedure were recorded at room temperature under the ×50 objective of a Renishaw System 1000 spectrometer. For 514.5 nm excitation, the power measured under the objective was *ca.* 4 mW, and a slit width of 5 μm was used. For 632.8 nm excitation, a slit width of 10 μm was used, and the power at the sample was *ca.* 6 mW for the MWCNs. This value was reduced to *ca.* 3 mW for the BCCNs in order to eliminate sample burning. The reported spectra are the average of ten accumulations. The spectra wavenumbers were calibrated by the superposition of Ne emission lines onto the spectra to give an accuracy of 1 cm^{-1}. Band centres and widths were obtained from Lorentzian fits to the observed band profiles.

3. EELS measurements

EELS analyses (Fig. 2) revealed the incorporation of boron into the hexagonal carbon network (B–C trigonal hybridisation at 188 eV). Boron is found frequently at the tips of the long tubes, and is also discernible in the nanotube walls. Nitrogen is completely absent. These results are consistent with a report[8] describing the aggregation of boron atoms at the opened ends

Fig. 1 TEM image of purified BCCNs.

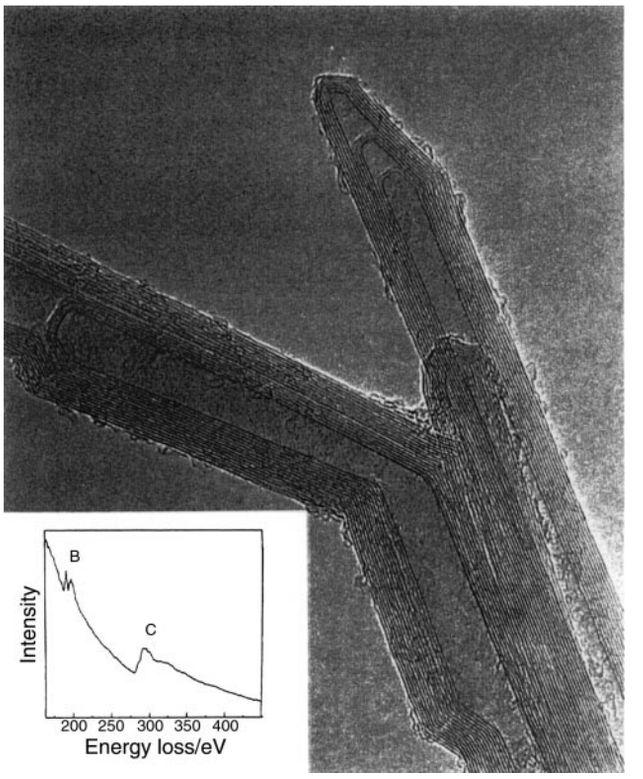

Fig. 2 EELS measurements performed at the tip region of individual BCCNs. Insert; the presence of BC_3 trigonal hybridisation at 188 eV $atom^{-1}$.

of growing tubes. However, we were unable to estimate the stoichiometry of BCCNs by EELS measurements, due to the broad distribution of tubule dimensions.

4. X-ray and electron diffraction measurements

a. In-plane structure

Due to curvature, the X-ray diffracting domains (*i.e.*, the coherent reflections resulting from the periodic atomic arrangements) of the carbon nanotubes are limited. For example, the *hk*0 reflections (*i.e.*, the in-plane reflections) arise as a result of axial (along the 100 and 110 axes) and non-axial reflections (angular and helical translational periodicities). In graphitic materials, *e.g.*, single graphite crystals or highly oriented pyrolytic graphite (HOPG), the reflections are equivalent along the *a*- and *b*-axes. For carbon nanotubes, the *hk*0 reflections are asymmetric (sawtoothed), indicating the presence of non-equivalent X-ray diffracting components, *i.e.*, the axial reflections are more intense than the non-axial reflections.[12] The BCCNs, which are of considerable length, are therefore expected to exhibit axial reflections that are stronger than those associated with MWCNs. In fact, we observed that the intensities of in-plane reflections are slightly weaker in BCCNs than in MWCNs (Fig. 3), particularly for the 110 reflection. This phenomenon may be due to the presence of localised BC_3 domains slightly influencing the periodic atomic arrangement of the hexagonal carbon network along the axis.

b. 3D ordering

The BCCNs also exhibit intense 3D ordering features, *e.g.*, the 101 reflection (similar to those of HOPG and a graphite single crystal; *i.e.*, due to hexagonal unit cell stacking) (Fig. 3). 3D ordering implies the presence of good alignment between the adjacent layers that make up the individual nanotubes.[13] MWCNs do not show discernible 3D ordering, due to the co-existence of helical and non-helical atomic arrangements in the tube walls.[14,15] It has been pointed out that the effect of boron at the open ends of growing tubes should result in preferential formation of a zigzag configuration.[8] In order to evaluate this prediction, micro-electron diffraction analyses were carried out on the individual BCCNs and BCCN bundles. Surprisingly, the zigzag pattern appeared frequently over several electron diffraction measurements (Fig. 4a and b), and is believed to represent the prevailing structure in the BCCN samples (the armchair, but not the helical patterns, were also observed). Dominant zigzag structures therefore seem to account for the observed 3D ordering feature (*i.e.*, a good alignment is present along the *c*-axis). Other reflections related to the orientation between layers, such as 102 and 112, can also be explained on the basis of the above description. Nevertheless, the question remains as to how an identical orientation (*i.e.*, zigzag edge) can be maintained in a concentric structure. For example, a four-layer carbon nanotube (*ca.*, 3 nm id) with constant separation of 0.34 nm would have circumferences: 3π nm,

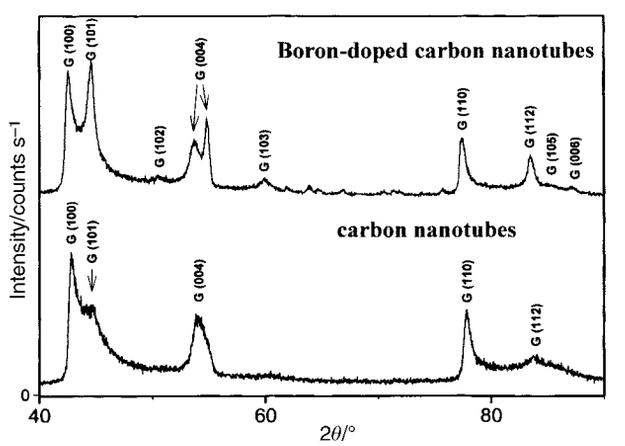

Fig. 3 X-ray diffraction patterns of BCCNs (top) and MWCNs (bottom), note that the 110 reflection is slightly weaker in BCCNs than in MWCNs.

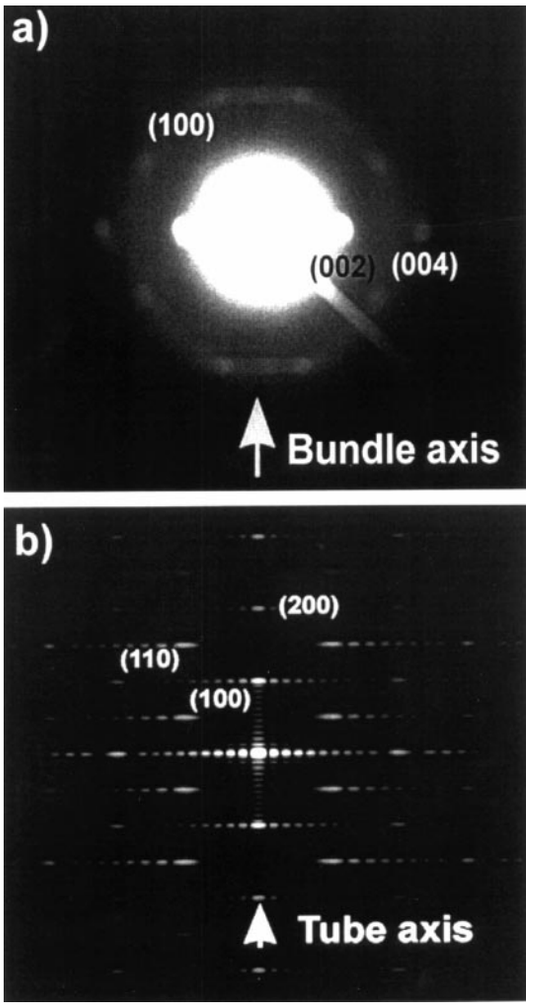

Fig. 4 Electron diffraction on individual BCCN bundles (a), consistent with the zigzag simulation (b).

$(0.34N_1+3)\pi$ nm, $(0.34N_2+3)\pi$ nm and $(0.34N_3+3)\pi$ nm from the innermost to the outermost layer ($N_1=2$, $N_2=4$, $N_3=6$). In a graphite sheet, the length of a hexagonal ring along the zigzag edge is 0.246 nm, so obviously the numbers of hexagonal rings in each shell are not integral (*i.e.*, 12.2, 14.9, 17.7 and 20.5). Moreover, the greater the number of the layers in a nanotube, the larger the gap between the rings in adjacent shells. In reality, alignment of carbon nanotube walls can be achieved in two ways: the variation of separation along the *c*-axis, or the formation of a polygonal cross-section. In practice, the varied 002 *d*-spacing in BCCNs has been observed by TEM.[7]

c. Finite crystal size along the *c*-axis

From the full width at half maximum (FWHM) analyses for the (002) peak and the Bragg equation, the number of graphite layers along the *c*-axis for BCCNs is *ca.* 42, comparable with that for MWCNs.[13] It is noteworthy (Fig. 3) that the 004 reflection is split, indicating the presence of varied *d*-spacing along the *c*-axis as the number of layer increases. This result is consistent with the TEM observations described above.

5. Vibrational spectroscopy

Partial replacement of carbon by boron in the nanotube structure will lower the local hexagonal symmetry and result in further IR-active vibrations. For N-doped graphite[16] analogous lowering of symmetry caused both the Raman D- and G-bands (*vide infra*) to become IR active, whereas we were unable to detect any IR absorption for our BCCN samples. This is probably because the BC_3 domains are localised on the nanotube tips, whilst the main contribution to the IR spectrum is expected to arise from the cylindrical sections of the tubes.[17] Nevertheless, the effects of boron doping were apparent in the Raman spectra of these samples.

The Raman spectrum of MWCNs, purified in the same way as the BCCNs, is shown in Fig. 5(a), 514.5 nm excitation, and is similar to previously reported spectra.[18,19] A strong band at 1571 cm^{-1}, corresponding to the E_{2g} G-band of HOPG, is downshifted by 9 cm^{-1} due to nanotube curvature.[20] The band width, 31 cm^{-1}, is slightly broader than that recorded for MWCNs (23 cm^{-1} [18] and 20–22 cm^{-1} [19]) and broader than that for HOPG (15 cm^{-1} [18,19]). A weak band, corresponding to the disorder-induced D-band of graphite, occurs at 1347 cm^{-1}. Hiura *et al.* attributed this band to the presence of nanometre-sized graphitic particles.[18] For crystalline graphite, the D-band : G-band intensity ratio ($I_D : I_G$) is inversely proportional to the crystal size in the direction of the graphite plane.[21] Kastner *et al.* used this relationship to estimate the average length of MWCNs, which was found to be between three and nine times less than the maximum bimodal length distribution obtained from an HRTEM study. They suggested that the D-band intensity is enhanced by nanotube curvature, tubes with smaller diameters providing the greater enhancement.[19] The intensity ratio (0.23) is larger than that measured here (0.06), although the tube diameters are similar in both studies. This outcome is probably due to the purification process, which results in the removal of large quantities of amorphous carbon and polyhedral carbon particles, thereby highlighting the characteristics of the nanotube structure.

The most intense absorption at high wavenumbers is the so-called (second order) D*-band, centred at 2687 cm^{-1} (bandwidth 82 cm^{-1}). Weak bands occur at 2445, 3147 and 3227 cm^{-1}. The broad 3147 cm^{-1} band has not been previously reported, and is probably the second order of the intense

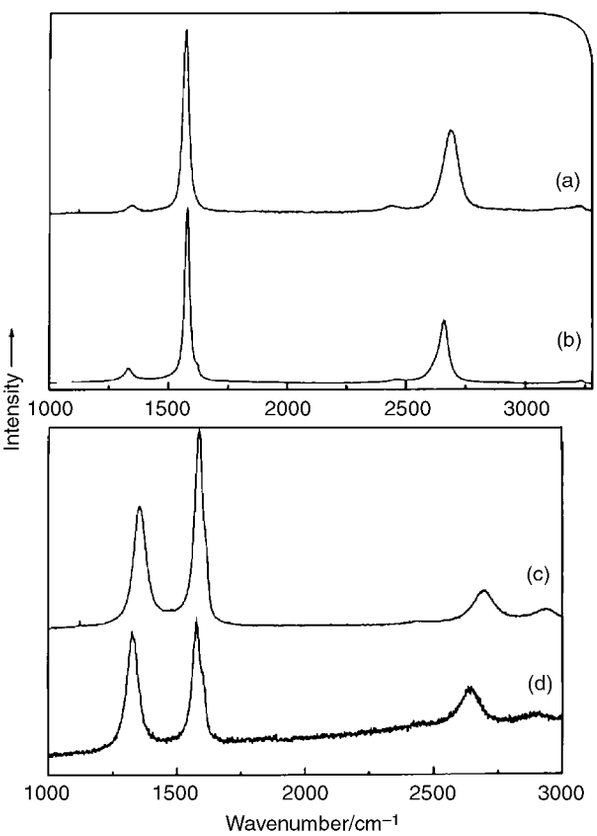

Fig. 5 Raman spectra of MWCNs with 514.5 nm (a) and 632.8 nm (b) excitation wavelengths. Raman spectra of BCCNs with 514.5 nm (c) and 632.8 nm (d) excitation wavelengths.

1571 cm^{-1} band. The other two bands were reported by Kastner *et al.*,[19] and are present in the graphite spectrum, where they are attributed to second-order features due to the contribution of a mid-Brillouin-zone extrema in the phonon density of states.[20]

The spectrum of MWCNs, excited with 632.8 nm radiation, is shown in Fig. 5(b). Although very similar to that recorded with 514.5 nm excitation, there are notable differences; *e.g.*, the $I_D : I_G$ ratio has increased from 0.06 at 514.5 nm to 0.10 at 632.8 nm. A similar change has been observed for various polycrystalline graphite and is attributed to resonance enhancement of the G-band upon excitation at shorter wavelengths; π–π* transition at 4–5 eV.[22] The appearance of a shoulder (1616 cm^{-1}) on the high wavenumber side of the G-band, was observed previously by Kastner *et al.* for both yellow and red nanotube excitations.[19] This band also occurs in the spectrum of graphite crystallites[23,24] and has been assigned to disorder-induced symmetry broken by the finite particle size, similar to the D-band. Another notable difference between the Raman spectra recorded with 514.5 and 632.8 nm excitation is that both the D- and D*-bands appear at lower wavenumbers with 632.8 nm excitation, the D- and D*-band being lowered by 14 cm^{-1} and 30 cm^{-1}, respectively. This phenomenon was noted by Kastner *et al.*,[19] who tentatively attributed the difference to phonon dispersion at the K and M derived points at the Brillouin-zone edge. Laser excitation then results in resonance enhancements of contributions from regions near to the observed D- and D*-bands.

Raman spectra of BCCNs are shown for 514.5 nm [Fig. 5(c)] and 632.8 nm [Fig. 5(d)] excitation. Below 1700 cm^{-1}, the BCCN bands are *ca.* 20% broader than the corresponding MWCN bands, the most obvious difference lying between their $I_D : I_G$ values. At 514.5 nm, the ratio increases from 0.06 for MWCNs to 0.90 for BCCNs, whilst at 632.8 nm it increases from 0.10 to 1.40. The high wavenumber shoulder on the G-band is evident for both excitation wavelengths in the spectra of BCCNs. These differences are consistent with the presence of boron atoms in the carbon framework, which reduce the ordering of the carbon atoms. Above 2500 cm^{-1}, the strongest D*-band is accompanied by a band at higher wavenumber. This is the D + G combination band ($1355 + 1583 = 2938$ cm^{-1}, seen at 2933 cm^{-1}, for the 514.5 nm line). Dispersion in the D- and D*-bands (and hence in the combination) is seen in the spectrum of the BCCNs. On going from 514.5 to 632.8 nm excitation, the D-band and D*-band are lowered by 28 and 55 cm^{-1}, respectively. This near doubling in the dispersion, proceeding from MWCNs to BCCNs, is related to differences in the electronic structure of these materials. Further interpretation of the electronic structure of BCCNs awaits detailed calculations.

Electron and X-ray diffraction analyses show that the BCCNs possess a well-defined 3D order, *i.e.*, the presence of boron does not significantly change the overall regularity of the hexagonal lattice in the nanotubes. Raman characterisation, on the other hand, is based on the nanotube vibrations, and is sensitive to departures from local hexagonal symmetry. This is apparent in the relatively intense D-band, which we have shown to be due to the presence of the BC_3 domains in the carbon framework, and does not reflect the actual crystallinity of the BCCNs.

6. The effect of boron on the electronic structure of carbon nanotubes

Microwave conductivity measurements on BCCN samples (Fig. 6) revealed a metallic profile in contrast to measurements on MWCNs which are characterisitic of thermally activated semi-conductors. For pure BC_3 nanotubes, calculations showed the presence of a free electron-like type structure, in

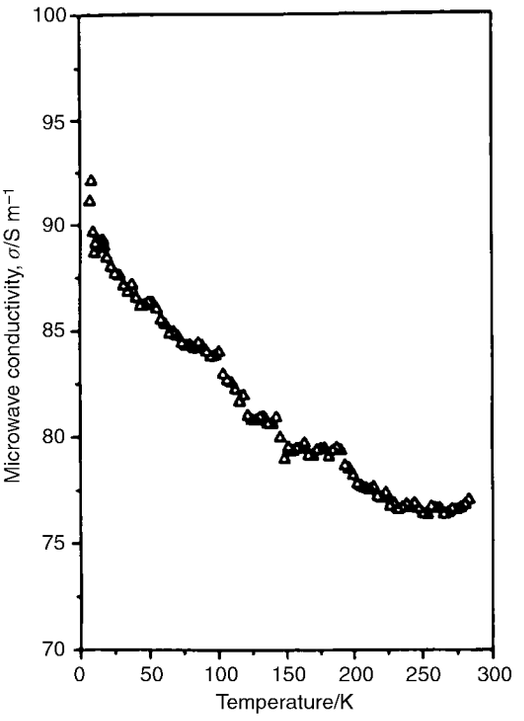

Fig. 6 Microwave conductivity measurements (11.8 GHz) of BCCNs, see also ref. 25.

which π and π* states (*i.e.*, conduction bands) located above the Fermi level intercept at the 2/3 position between the Γ and X points in the Brillouin zone.[26] However, the electronic structure of BCCNs resembles that predicted by classic band theory for silicon-based semi-conductors (*i.e.*, an extra energy level is created near the valence band edge as a P-type dopant is introduced), since the carbon nanotubes are partly doped with boron.

The introduction of boron into carbon networks increases the number of (hole-type) charge carriers, thus enhancing conductivity. Nevertheless, the BC_3 units also act as structure defects, resulting in an increase in scattering density and therefore a lowering of the carrier mobility. However, as EELS investigations indicated that the BC_3 domains are mainly confined to the tip regions of the tubes, the scattering density increment along the in-plane direction may not be significant in BCCNs.

The BC_3 domains are more likely to be present in the outer than in the inner layers. Experiments, performed by Carroll *et al.*, using STM to analyse directly the local density of states (LDOS) on the individual BCCNs, showed the disappearance of the band gap over the BC_3 domains.[27] This fact supports our assumption (*vide supra*). Meanwhile, if greater energy is required for pentagonal ring formation in the presence of boron at the open edge of the tube, one should expect that the energy requirement is much greater in the inner than in the outer layers, due to the presence of greater strain in the inner layers.

In summary, the introduction of boron into carbon nanotubes results in: (a) increase in 3D ordering, due to the presence of good alignment along the *c*-axis, but slightly less ordering in the in-plane direction of the nanotubes, caused by the reduction of hexagonal lattice regularity; (b) hexagonal lattice symmetry breaking, due to the formation of BC_3 units; and (c) enhancement of nanotube conductivity.

Acknowledgements

We thank the EPSRC (WKH), the JFCC (YQZ), the Royal Society (NG), ULIRS (SF, RJHC), the CONACYT-México

25237 (HT), the DGAPA-UNAMES 107-296 (HT) and the Mexican Academy of Science (HT) for financial support. J. Thorpe and D.P. Randall (Sussex) provided valuable assistance with the electron microscopy.

References

1 J. A. Turnbull, M. S. Stagg and W. T. Eeles, *Carbon*, 1966, **3**, 387.
2 C. E. Lowell, *J. Am. Ceram. Soc.*, 1967, **50**, 142.
3 P. Wagner and L. M. Dickinson, *Carbon*, 1970, **8**, 313.
4 *Chemistry and Physics of Carbon*, ed. P. A. Thrower, 1965, vol. 19, pp. 3–28.
5 O. Stephan, P. M. Ajayan, C. Colliex, Ph. Redlich, J. M. Lambert, P. Bernier and P. Lefin, *Science*, 1994, **266**, 1683.
6 Ph. Redlich, J. Loeffler, P. M. Ajayan, J. Bill, F. Aldinger and M. Rühle, *Chem. Phys. Lett.*, 1996, **260**, 465.
7 M. Terrones, W. K. Hsu, S. Ramos, R. Castillo and H. Terrones, *Fullerene Sci. Nanotechnol.*, 1998, **6**, 787.
8 B. C. Satishkumar, A. Govindaraj, K. R. Harikumar, J. P. Zhang, A. K. Cheetham and C. N. Rao, *Chem. Phys. Lett.*, 1999, **300**, 473.
9 X. Blase, J.-C. Charlier, A. De Vita, R. Car, Ph. Redlich, M. Terrones, W. K. Hsu, H. Terrones, D. L. Carroll and P. M. Ajayan, *Phys. Rev. Lett.*, 1999, **83**, 5078.
10 K. B. Shelimov, R. O. Esenaliev, A. G. Rinzler, C. B. Huffman and R. E. Smalley, *Chem. Phys. Lett.*, 1998, **282**, 429.
11 T. W. Ebbesen, P. M. Ajayan, H. Hiura and K. Tanigaki, *Nature*, 1994, **367**, 519.
12 D. Reznik, C. H. Olk, D. A. Neumann and J. R. D. Copley, *Phys. Rev. B*, 1995, **52**, 116.
13 M. Terrones, J. P. Hare, W. K. Hsu, H. W. Kroto, A. Lappas, W. K. Maser, A. J. Pierik, K. Prassides, R. Taylor and D. R. M. Walton, *Proceedings of the Symposium on the Related Advanced in Chemistry and Physics of Fullerenes and Related Materials, May, Reno (USA)*, ed. R. S. Ruoff and K. M. Kadish, The Electrochemical Society, Pennington, NJ, 1995, p. 599.
14 M. Liu and J. M. Cowley, *Carbon*, 1993, **31**, 393.
15 M. Liu and J. M. Cowley, *Carbon*, 1995, **33**, 225.
16 J. H. Kaufman, S. Metin and D. D. Saperstein, *Phys. Rev. B*, 1989, **39**, 13053.
17 M. S. Dresselhaus, G. Dresselhaus and R. Saito, *Phys. Rev. B*, 1992, **45**, 6234.
18 H. Hiura, T. W. Ebbesen, K. Tanigaki and H. Takahashi, *Chem. Phys. Lett.*, 1993, **202**, 509.
19 J. Kastner, T. Pichler, H. Kuzmany, S. Curran, W. Blau, D. N. Weldon, M. Delamesiere, S. Draper and H. Zandbergen, *Chem. Phys. Lett.*, 1994, **221**, 53.
20 W. S. Bacsa, W. A. de Heer, D. Ugarte and A. Chatelain, *Chem. Phys. Lett.*, 1993, **211**, 346.
21 F. Tuinstra and J. L. Koenig, *J. Chem. Phys.*, 1970, **53**, 1126.
22 K. Sinha and J. Menendez, *Phys. Rev. B*, 1990, **41**, 10845.
23 R. P. Vidano, D. B. Fischbach, J. Willis and T. H. Loer, *Solid State Commun.*, 1981, **39**, 341.
24 K. Nakamura, M. Fujitsaka and M. Kitajima, *Phys. Rev. B*, 1990, **41**, 12260.
25 M. Terrones, W. K. Hsu, A. Schilder, H. Terrones, N. Grobert, J. P. Hare, Y. Q. Zhu, M. Schwoerer, K. Prassides, H. W. Kroto and D. R. M. Walton, *Appl. Phys. A*, 1998, **66**, 307.
26 Y. Miyamoto, A. Rubio, S. G. Louie and M. L. Cohen, *Phys. Rev. B*, 1994, **50**, 18360.
27 D. L. Carroll, Ph. Redlich, X. Blase, J.-C. Charlier, S. Curran, P. M. Ajayan, S. Roth and M. Rühle, *Phys. Rev. Lett.*, 1998, **81**, 2332.